Supporting Online Material for

Bistability in Atomic-Scale Antiferromagnets

Sebastian Loth,* Susanne Baumann, Christopher P. Lutz, D. M. Eigler, Andreas J. Heinrich*

*To whom correspondence should be addressed. E-mail: heinrich@almaden.ibm.com (A.J.H.); sebastian.loth@mpsd.cfel.de (S.L.)

Published 13 January 2012, *Science* **335**, 196 (2012)
DOI: 10.1126/science.1214131

This PDF file includes:

Materials and Methods

Sample preparation

All experiments were performed in a low-temperature STM equipped with a variable magnetic field. Cu(100) single crystals were cleaned by repeated Ar sputter-anneal cycles. One monolayer of Cu_2N was formed by nitrogen ion bombarding the clean Cu(100) near room temperature, and subsequent annealing to about 300 °C *(32)*. Fe atoms were deposited onto the cold sample surface at 4.2 K with a density of ~1% of a monolayer.

Fe atoms were positioned 0.72 nm apart on the two-fold symmetric Cu binding sites of the Cu_2N overlayer using vertical atom manipulation *(20, 33, 34)*. Surface and spacing were chosen to give magnetic coupling that is adequate to demonstrate antiferromagnetism, while keeping the atoms well enough separated to clearly resolve the location and spin state of each one. For atom pick-up, the probe tip was lowered close to point-contact (~100 kΩ junction resistance) and a sample voltage of +1.7 V was applied while withdrawing the tip. Drop-off employed a two-step process in which the atom was first positioned atop a nitrogen surface atom (N-binding site) by lowering the loaded tip into point-contact and withdrawing at zero voltage, and subsequently the dropped atom was hopped laterally to a Cu binding site with a +0.75 V voltage pulse with the tip positioned laterally to guide the atom to the intended binding site.

Spin polarized tips

Spin-polarized tips were created by transferring one or more magnetic atoms (Fe or Mn) from the surface to the apex of the tip *(34)*. Such a tip behaves like a paramagnet and gives spin-polarized tunnel currents at < 10 K when external magnetic fields of >0.5 T are applied. The degree of spin-polarization of the tips was determined from measurements on isolated Fe and Mn atoms *(34)*. Using the customary definition of the spin-polarization *(38)*, η, we determined $\eta = 0.6$ for the tip used in Fig. 1 and $\eta = 0.3$ for the tip in Fig. 4. Tips with reverse spin-polarization (anti-aligned to the magnetic field) were produced by placing more than one magnetic atom at the apex, the atoms presumably coupling to each other antiferromagnetically. Tips that show net spin-polarization at 0 T magnetic field were produced by attaching >10 Fe atoms at the tip apex. The magnetic contrast does not depend significantly on the magnitude or sign of the applied voltage as long as the junction voltage is small enough (~5 mV) to avoid disrupting the spin state of the AFM structure. Since a large fraction of the tunnel current is spin dependent for Fe atoms on this surface, we typically observe a large (factor-of-two) change in conductance.

Exchange coupling analysis

The nearest-neighbor exchange coupling constants, J and J', were determined from spin excitation spectroscopy *(35)* of Fe dimers shown in Fig. S1. Spectra of dimers on this surface have previously been described with a spin Hamiltonian that includes Zeeman energy, uniaxial and transverse anisotropy and isotropic Heisenberg exchange interaction *(36)*.

Because the exchange coupling energies for the 0.72 nm spaced dimers are weaker than the easy-axis anisotropy energy of each Fe atom we can replace Heisenberg

interaction with Ising spin coupling and assume that transverse anisotropy is negligible. This use of Ising spin coupling results in a diagonal spin Hamiltonian H, which simplifies the fitting of the exchange coupling constants significantly. We verified that use of the full spin Hamiltonian produces only small corrections to the fitted coupling constants. We use

$$H = JS_{1,z} \cdot S_{2,z} + \sum_{i=1,2} H_i$$

$$H_i = g\mu_B B_z S_{i,z} + D S_{i,z}^2$$

where $S_{i,z}$ is the z-component of the spin operator for Fe atom i, g the Landé g-factor, B_z the applied magnetic field, and D the uniaxial anisotropy parameter.

For the dimer assembled along the N row (Fig. S1A) the second derivative of the tunnel current $d^2I/dV^2(V)$ shows two prominent spin excitations as peaks at positive voltage and corresponding dips at negative voltage *(37)*. Both excitations are at higher energy than the prominent spin excitation observed for an isolated reference Fe atom. By fitting the above spin Hamiltonian, H, to these excitation energies we obtain $J = 1.3 \pm 0.1$ meV. The stated error represents variations in J found on different dimers.

For the dimer assembled perpendicular to the N rows (Fig. S1B) we find only one spin excitation at slightly lower energy than that of the reference Fe. Fitting the spin Hamiltonian, H, yields $J' = 0.03 \pm 0.02$ meV.

We note that the small energy shifts of ~60 μeV are approaching the achievable accuracy of spin excitation spectroscopy acquired at 0.5 K and in the presence of variations due to different local environment. Therefore we verified the magnitude of J' by comparing it to the Zeeman energy (which only depends on the g factor and the magnetic field). At high fields the Zeeman energy dominates the weak exchange coupling J' between chains, whereas at low fields the J' dominates over the Zeeman energy.

Switching rate analysis

Rates slower than 10^3 s^{-1} in Figs. 2, 3 and S3 were found by using constant-V (non-pulsed) current traces and taking the reciprocal of the mean time in each state. In order to measure current-induced switching at higher voltages (Fig. 2) where the switching rates are faster than the 1 kHz bandwidth of the current amplifier used to detect the magnetic states, we applied the switching voltage in brief pulses, and monitored the state of the structure after each pulse using a low voltage, i.e. a voltage below the threshold for switching (Fig. 2B). Switching rates were determined from the measured probabilities of switching due to each pulse, under the assumption that there are only two magnetic states and that transitions in each direction occur with fixed probabilities per unit time during application of the pulse. This assumption was checked by measuring with different pulse widths w for each point and finding no change in rates, within statistical uncertainty. When the average time between switching events approaches the pulse width, multiple transitions are likely to occur during a single pulse. This effect was taken into consideration as follows. The magnetic state was measured after each of n pulses having pulse width w. Let n_i be the number of pulses starting in state i, and n_{ij} the number of transitions from state i to j. The best estimates of the steady-state probabilities of occupying each state are $p_i = n_i / n$, and probabilities of transition between states due to one pulse are $q_{ij} = n_{ij} / n_i$. Then, the transition rate to state j, when starting from state i, is then given by $\rho_{ij} = -(q_{ij}/w) \times \ln(1 - q_s)/q_s$, where we define $q_s = q_{01} + q_{10}$.

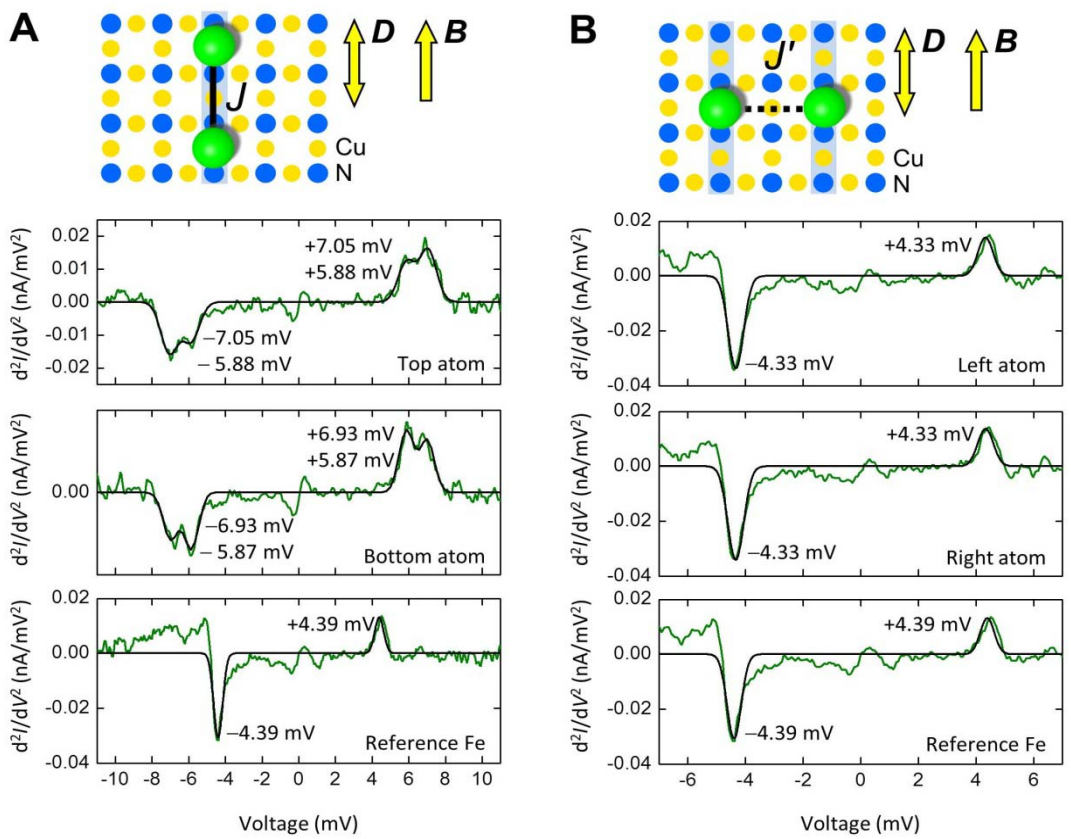

Fig. S1.

Measurement of nearest-neighbor exchange coupling energies J and J'. The symmetry of the Cu_2N surface provides two distinctly different coupling geometries for a spacing of 0.72 nm: parallel and perpendicular to nitrogen rows. The exchange coupling is found to be a factor 40 stronger along the N row. **A** Top panel: Sketch of a Fe dimer (green) coupled along one row of N (blue) and Cu (yellow) atoms. Anisotropy axis, D, and applied magnetic field, B, are parallel to the N row. Bottom panels: Spin excitation spectra recorded over the top and bottom atom of the dimer and a reference Fe atom on the same surface. **B** Top panel: Sketch of a dimer coupled perpendicular to the N rows. Bottom panels: corresponding spin excitation spectra for the dimer and the reference atom. Spectra are plotted as d^2I/dV^2, the second derivative of the tunnel current, in which a spin excitation at eV energy is identified as a dip at voltage $-V$ and a peak at $+V$. Measured curves (green lines) were fitted with one or two double Gaussian functions with centers constrained to be symmetric around $V = 0$ *(37)*. Fitted spin excitation voltages are printed in the graphs and coupling constants, J, J', calculated using the spin Hamiltonian, H, described above.

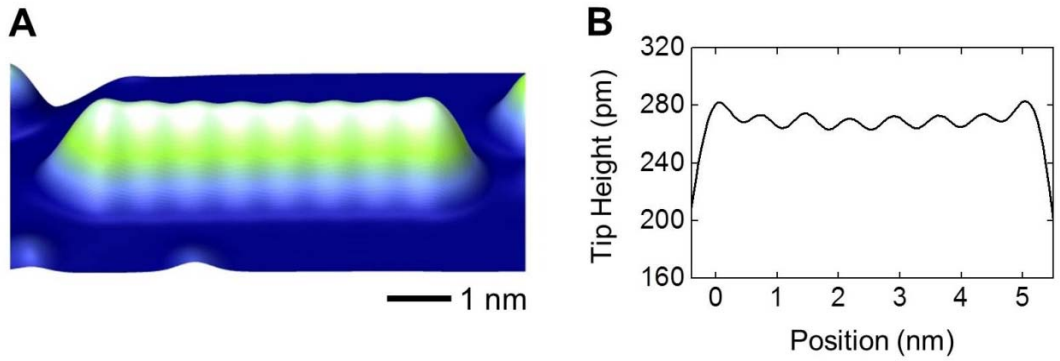

Fig. S2

Arrays of coupled Mn atoms. **A** STM image of a linear chain of 8 Mn atoms with 0.72 nm spacing between the atoms that was constructed by atom manipulation analogous to the Fe arrays. Image recorded at 3 T magnetic field and 1.2 K temperature with a probe tip having strong spin polarization, $\eta = 0.7$. Voltage 2 mV, current 25 pA. **B** Section through center of the chain. No bistability could be observed and no magnetic order was clearly discernable. The chain ends show possible weak antiferromagnetic contrast with <4 pm height variation from atom to atom, compared to >40 pm modulation for a (1×8) Fe chain (Fig. 1C,E).

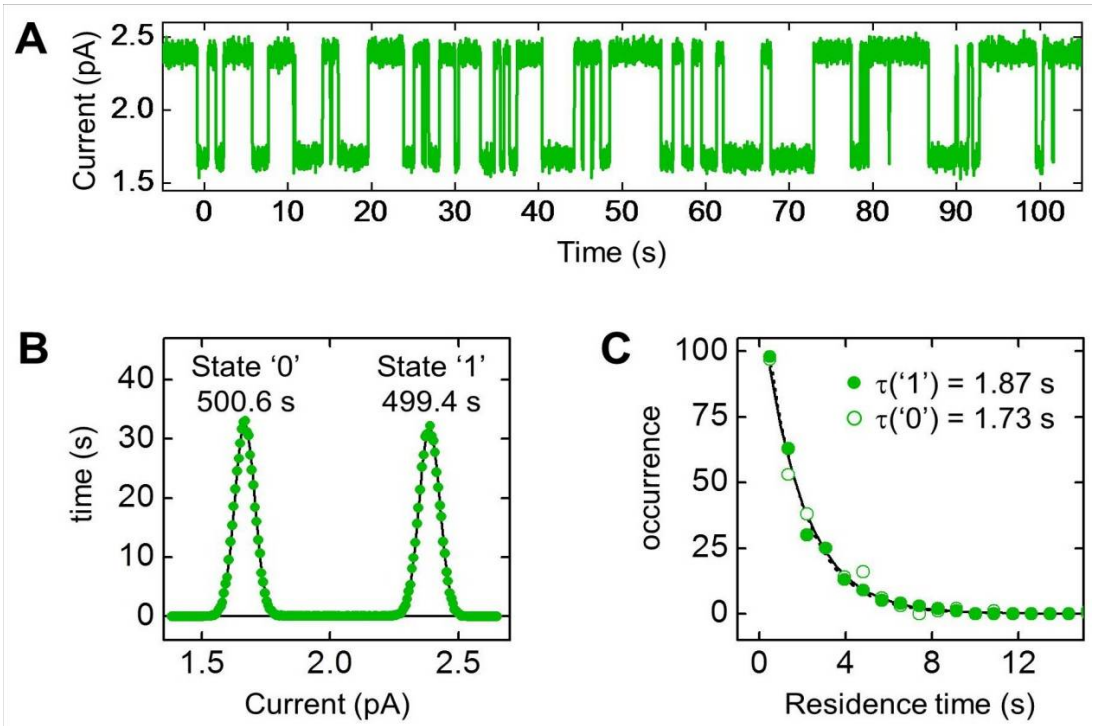

Fig. S3

Thermally activated switching of an antiferromagnetic array. **A** Two-state noise recorded on (2 × 6) Fe-array of Fig. 3A at 4.75 K temperature and 3 T magnetic field. Tip position fixed over third atom from top at 2 mV, 2 pA. **B** Histogram of tunnel current for 1000 s of recording (bin size 6.4 fA) showing that the (2 × 6) Fe-array switches between two states and resides equal amounts of time in either state. This shows that the two states are degenerate and that the AFM structure is fully spin compensated. **C** Histogram of residence times in each state measured by the time between two switching events (bin size 0.51 s). Filled circles show state '1' with mean residence time $\tau('1') = 1.87$ s determined as the 1/e decay constant of a single exponential decay function fitted to the histogram (solid line). Open circles show state '0' and fit (dashed line) with $\tau('0') = 1.73$ s. This analysis is repeated for different temperatures and magnetic fields (1 T and 3 T). Fig. 3E presents resulting mean switching rates as $(\frac{1}{2}\,[\tau('1') + \tau('0')])^{-1}$.

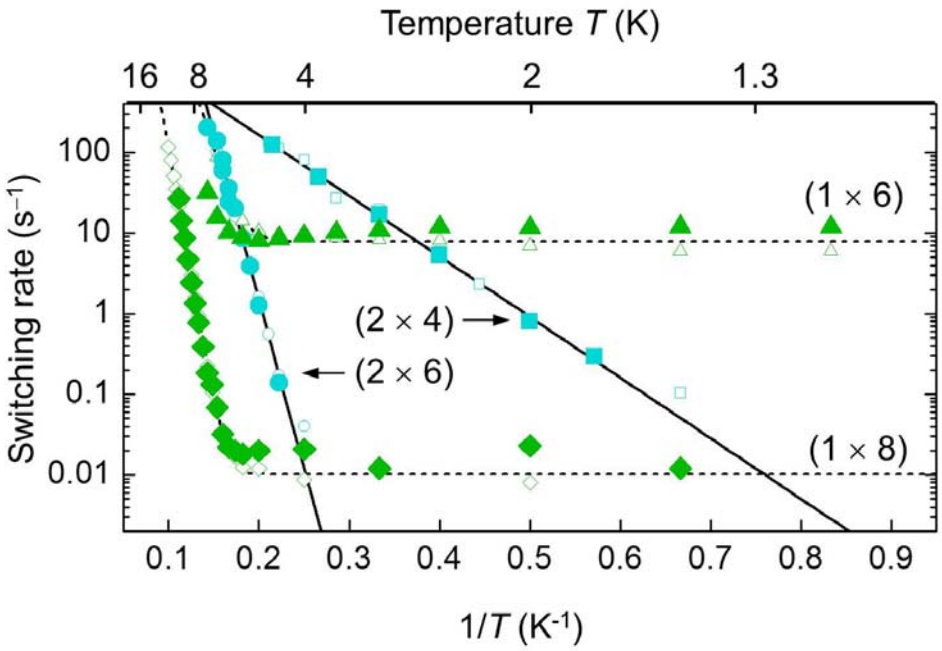

Fig. S4

Magnetic field dependence of the thermal stability of antiferromagnetic arrays. Filled symbols show switching rates for the different arrays at 1 T magnetic field (open symbols show 3 T data repeated from Fig. 3). Fit curves repeated from Fig. 3. Structures (2 × 6), (2 × 4) and (1 × 8) show no dependence on the magnetic field. Only the (1 × 6) chain changes its high temperature switching behavior to slightly lower switching rates for T > 6 K.

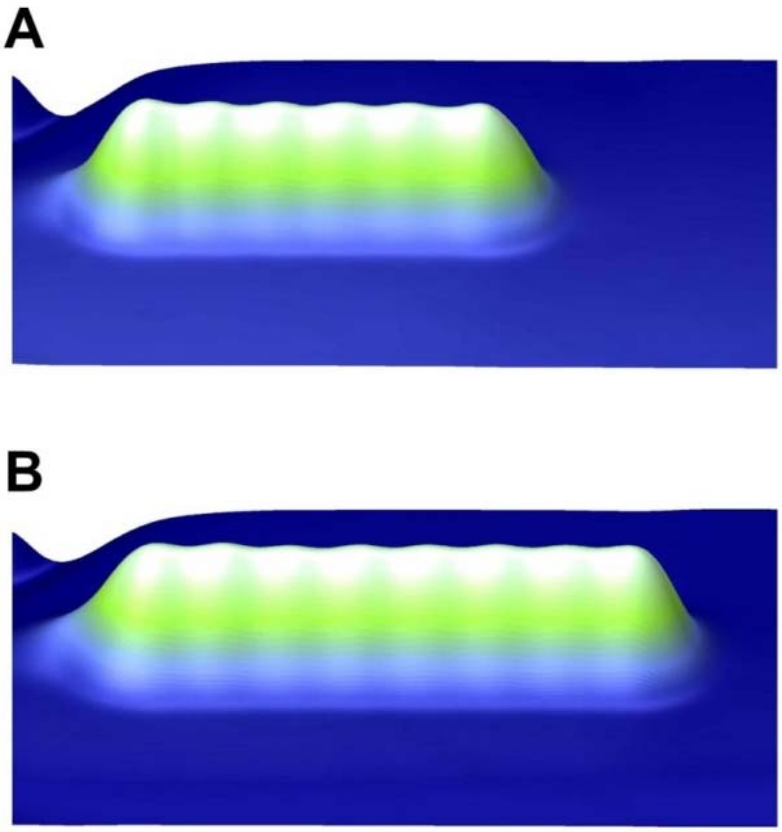

Fig. S5

STM images of Fe atom arrays. (**A**) A linear chain of 6 Fe atoms with 0.72 nm spacing between the atoms. This chain is labeled (1 × 6) chain in the text. (**B**) A (1 × 8) chain that was constructed by adding two Fe atoms to the chain of A. Image recorded with a probe tip having only very weak spin polarization, size 8.2 × 5.2 nm^2, green is high and blue is low. Voltage 2 mV, current 10 pA.

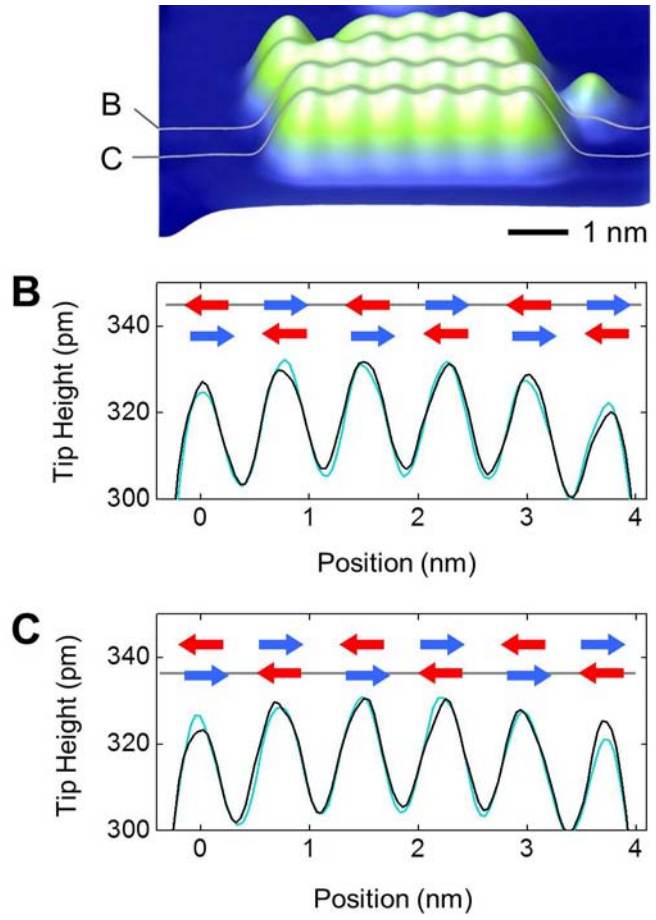

Fig. S6

Néel order of (2×6) Fe array in zero magnetic field. **A** STM image of (2×6) Fe array (front). Image recorded at 0 T magnetic field and 1.2 K temperature with a spin-polarized tip. Grey lines indicate sections through the array. **B** Section through the center of the top row of Fe atoms for Néel state '1' (black line) and Néel state '0' (blue line). Comparison of state '1' and state '0' reveals alternating height contrast demonstrating stable Néel order at 0 T (amplitude ~3pm on the corner atoms). **C** Section through the center of the bottom row of Fe atoms (same color scale). Comparison of state '1' and '0' also shows alternating order but inverted to that in panel B as expected for Néel order throughout the array. Same procedure used for sections of Néel state '0'.The array could be switched in the same manner as described in Fig. 2 of the main text. The additional Fe atoms (back part) are part of an incomplete second magnetic bit, with the two bits being magnetically decoupled as discussed in Fig. 4. A small amount of spin polarization of the tip at 0 T parallel to the easy axis of the Fe atoms was achieved by transferring >10 Fe atoms to the tip apex.

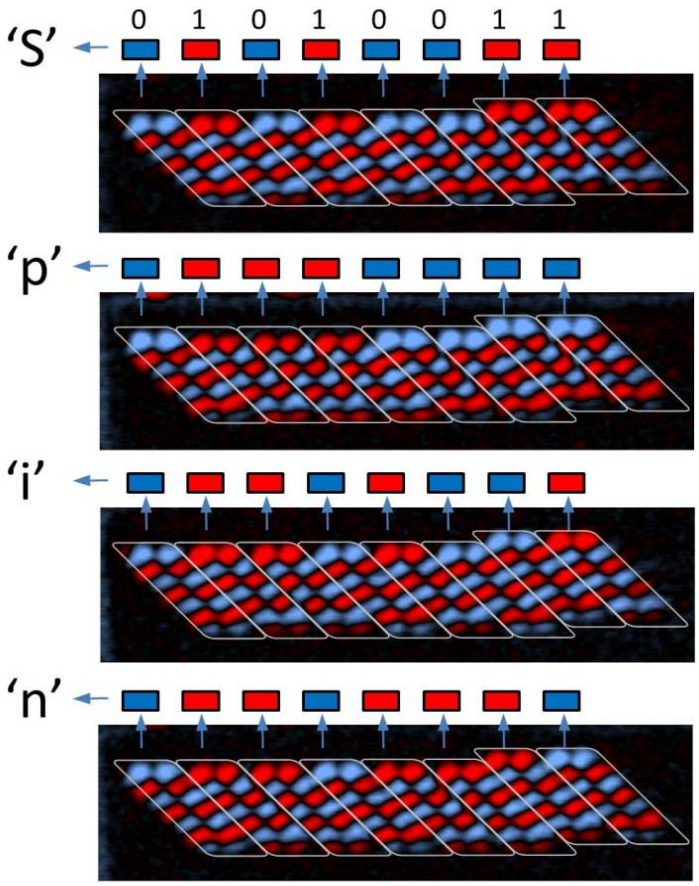

Fig. S7

Dense magnetic data storage. The binary representation of the characters "S,p,i,n" were stored in the AFM byte of Fig. 4 and read by imaging at 2 mV voltage and 1 pA tunnel current. Each (2×6) array represents a '1' when its top atoms are parallel to the tip's spin-polarization (red) and '0' when the top atoms are anti-aligned (blue). Data displayed similar to Fig. 4C as the difference between the spin-polarized and spin-averaged topography.

Array size	Prefactor ρ_0 (s^{-1})	Energy barrier E_B (meV)	Tunneling Rate ρ_T (s^{-1})
(1 × 6)	3×10^{7}	7.2 ± 1.1	7.86
(1 × 8)	2×10^{8}	12.3 ± 0.1	0.01
(2 × 4)	5×10^{3}	1.5 ± 0.1	--
(2 × 6)	3×10^{8}	8.2 ± 0.2	--

Table S1.
Fit parameters for switching rates of Fig. 3E. The modified Arrhenius function $\rho = \rho_0 \cdot \exp(-E_B/k_B T) + \rho_T$ (with ρ_T: temperature independent tunneling rate) is fitted to the temperature-dependent switching rates of each structure.

References and Notes

1. C. Chappert, A. Fert, F. N. Van Dau, The emergence of spin electronics in data storage. *Nat. Mater.* **6**, 813 (2007). doi:10.1038/nmat2024 Medline

2. R. Wiesendanger, H.-J. Güntherodt, G. Güntherodt, R. J. Gambino, R. Ruf, Observation of vacuum tunneling of spin-polarized electrons with the scanning tunneling microscope. *Phys. Rev. Lett.* **65**, 247 (1990). doi:10.1103/PhysRevLett.65.247 Medline

3. J. W. Lau, J. M. Shaw, Magnetic nanostructures for advanced technologies: fabrication, metrology and challenges. *J. Phys. D Appl. Phys.* **44**, 303001 (2011). doi:10.1088/0022-3727/44/30/303001

4. J. V. Barth, G. Costantini, K. Kern, Engineering atomic and molecular nanostructures at surfaces. *Nature* **437**, 671 (2005). doi:10.1038/nature04166 Medline

5. G. Herzog, S. Krause, R. Wiesendanger, Heat assisted spin torque switching of quasistable nanomagnets across a vacuum gap. *Appl. Phys. Lett.* **96**, 102505 (2010). doi:10.1063/1.3354023

6. S. Krause *et al*., Magnetization reversal of nanoscale islands: How size and shape affect the arrhenius prefactor. *Phys. Rev. Lett.* **103**, 127202 (2009). doi:10.1103/PhysRevLett.103.127202 Medline

7. P. Gambardella *et al*., Ferromagnetism in one-dimensional monatomic metal chains. *Nature* **416**, 301 (2002). doi:10.1038/416301a Medline

8. J. D. Rinehart, M. Fang, W. J. Evans, J. R. Long, Strong exchange and magnetic blocking in N_2^{3-}-radical-bridged lanthanide complexes. *Nat. Chem.* **3**, 538 (2011). doi:10.1038/nchem.1063 Medline

9. L. Thomas *et al*., Macroscopic quantum tunnelling of magnetization in a single crystal of nanomagnets. *Nature* **383**, 145 (1996). doi:10.1038/383145a0

10. J. R. Friedman, M. P. Sarachik, J. Tejada, R. Ziolo, Macroscopic measurement of resonant magnetization tunneling in high-spin molecules. *Phys. Rev. Lett.* **76**, 3830 (1996). doi:10.1103/PhysRevLett.76.3830 Medline

11. F. Nolting *et al*., Direct observation of the alignment of ferromagnetic spins by antiferromagnetic spins. *Nature* **405**, 767 (2000). doi:10.1038/35015515 Medline

12. S. Heinze *et al*., Real-space imaging of two-dimensional antiferromagnetism on the atomic scale. *Science* **288**, 1805 (2000). doi:10.1126/science.288.5472.1805 Medline

13. C. L. Gao, W. Wulfhekel, J. Kirschner, Revealing the 120 degrees antiferromagnetic Néel structure in real space: One monolayer Mn on Ag(111). *Phys. Rev. Lett.* **101**, 267205 (2008). doi:10.1103/PhysRevLett.101.267205 Medline

14. U. Kaiser, A. Schwarz, R. Wiesendanger, Magnetic exchange force microscopy with atomic resolution. *Nature* **446**, 522 (2007). doi:10.1038/nature05617 Medline

15. I. E. T. Iben, in *31st EOS/ESD Symposium* (ESD Association, Rome, NY, 2009), p. 1.

16. X. Chen, A. Hochstrat, P. Borisov, W. Kleemann, Magnetoelectric exchange bias systems in spintronics. *Appl. Phys. Lett.* **89**, 202508 (2006). doi:10.1063/1.2388149

17. A. V. Kimel *et al*., Inertia-driven spin switching in antiferromagnets. *Nat. Phys.* **5**, 727 (2009). doi:10.1038/nphys1369

18. Supporting material is available on *Science* Online.

19. C. F. Hirjibehedin *et al*., Large magnetic anisotropy of a single atomic spin embedded in a surface molecular network. *Science* **317**, 1199 (2007). doi:10.1126/science.1146110 Medline

20. C. F. Hirjibehedin, C. P. Lutz, A. J. Heinrich, Spin coupling in engineered atomic structures. *Science* **312**, 1021 (2006). doi:10.1126/science.1125398 Medline

21. O. Waldmann, T. Guidi, S. Carretta, C. Mondelli, A. L. Dearden, Elementary excitations in the cyclic molecular nanomagnet Cr8. *Phys. Rev. Lett.* **91**, 237202 (2003). doi:10.1103/PhysRevLett.91.237202 Medline

22. I. Bose, A. K. Pal, Motion of bound domain walls in a spin ladder. *Eur. Phys. J. B* **77**, 139 (2010). doi:10.1140/epjb/e2010-00240-1

23. A. A. Khajetoorians, J. Wiebe, B. Chilian, R. Wiesendanger, Realizing all-spin-based logic operations atom by atom. *Science* **332**, 1062 (2011). doi:10.1126/science.1201725 Medline

24. P. M. Haney, R. A. Duine, A. S. Núñez, A. H. MacDonald, Current-induced torques in magnetic metals: Beyond spin-transfer. *J. Magn. Magn. Mater.* **320**, 1300 (2008). doi:10.1016/j.jmmm.2007.12.020

25. S. Urazhdin, N. Anthony, Effect of polarized current on the magnetic state of an antiferromagnet. *Phys. Rev. Lett.* **99**, 046602 (2007). doi:10.1103/PhysRevLett.99.046602 Medline

26. S. Loth, M. Etzkorn, C. P. Lutz, D. M. Eigler, A. J. Heinrich, Measurement of fast electron spin relaxation times with atomic resolution. *Science* **329**, 1628 (2010). doi:10.1126/science.1191688 Medline

27. S. Mørup, D. E. Madsen, C. Frandsen, C. R. H. Bahl, M. F. Hansen, Experimental and theoretical studies of nanoparticles of antiferromagnetic materials. *J. Phys. Condens. Matter* **19**, 213202 (2007). doi:10.1088/0953-8984/19/21/213202

28. W. Wernsdorfer *et al*., Macroscopic quantum tunneling of magnetization of single ferrimagnetic nanoparticles of barium ferrite. *Phys. Rev. Lett.* **79**, 4014 (1997). doi:10.1103/PhysRevLett.79.4014

29. D. Gatteschi, R. Sessoli, J. Villain, *Molecular Nanomagnets* (Oxford Univ. Press, New York, 2006).

30. B. Barbara, E. M. Chudnovsky, Macroscopic quantum tunneling in antiferromagnets. *Phys. Lett. A* **145**, 205 (1990). doi:10.1016/0375-9601(90)90682-E

31. E. E. Fullerton *et al.*, Antiferromagnetically coupled magnetic media layers for thermally stable high-density recording. *Appl. Phys. Lett.* **77**, 3806 (2000). doi:10.1063/1.1329868

32. F. Komori, S.-Y. Ohno, K. Nakatsuji, Lattice deformation and strain-dependent atom processes at nitrogen-modified Cu(001) surfaces. *Prog. Surf. Sci.* **77**, 1 (2004). doi:10.1016/j.progsurf.2004.06.002

33. L. Bartels, G. Meyer, K.-H. Rieder, Controlled vertical manipulation of single CO molecules with the scanning tunneling microscope: A route to chemical contrast. *Appl. Phys. Lett.* **71**, 213 (1997). doi:10.1063/1.119503

34. S. Loth, C. P. Lutz, A. J. Heinrich, Spin-polarized spin excitation spectroscopy. *New J. Phys.* **12**, 125021 (2010). doi:10.1088/1367-2630/12/12/125021

35. A. J. Heinrich, J. A. Gupta, C. P. Lutz, D. M. Eigler, Single-atom spin-flip spectroscopy. *Science* **306**, 466 (2004). doi:10.1126/science.1101077 Medline

36. A. F. Otte *et al.*, Spin excitations of a Kondo-screened atom coupled to a second magnetic atom. *Phys. Rev. Lett.* **103**, 107203 (2009). doi:10.1103/PhysRevLett.103.107203 Medline

37. J. Lambe, R. C. Jaklevic, Molecular vibration spectra by inelastic electron tunneling. *Phys. Rev.* **165**, 821 (1968). doi:10.1103/PhysRev.165.821

38. R. Wiesendanger, Spin mapping at the nanoscale and atomic scale. *Rev. Mod. Phys.* **81**, 1495 (2009). doi:10.1103/RevModPhys.81.1495